Supramolecular Gels for Antimicrobial Photodynamic Therapy against *E. coli* and *S. aureus*

ABSTRACT:

Singlet oxygen (SO) reacts with organic molecules, for example in degrading environmental contaminants and causing toxicity to cells in photodynamic therapy (PDT). The relevance of SO in the environmental and biomedical domains has fuelled research towards improved methodologies for its efficient generation. In this paper, we report the use of a bis-imidazolium-based amphiphile that forms supramolecular gels in water-ethanol mixtures encapsulating SO generating chromophores. The gels comprise twisted fibres that incorporate one of four different porphyrins: 5,10,15,20-tetrakis(*N*-methyl-4-pyridinium)porphyrin tetraiodide (TPPP), 5,10,15,20-tetrakis(4-carboxyphenyl)porphyrin (TCPP), 5,10,15,20-tetrakis(3-hydroxyphenyl)porphyrin (TPP-3OH) and 5,10,15,20-tetrakis(4-hydroxyphenyl)porphyrin (TPP-4OH). Rheological measurements confirmed viscoelastic properties characteristic of these types of supramolecular gels, suggesting their potential as effective local PDT delivery systems. Enhanced SO generation within the hydrogel matrix compared to the solution of the chromophores was observed in suspension in a spectrophotometer using uric acid as the molecular probe. The SO generation was also shown through antimicrobial PDT (aPDT) studies. The TPPP-containing gel showed the highest reduction in the colony forming unit (CFU) count, which is 94% against *E. coli* and 100% against *S. aureus*. These results indicate that the porphyrin gels based on a gemini amphiphile with a high level of SO production are of significant interest and have a lot of potential use in aPDT.

Keywords**:** Singlet oxygen**,** Supramolecular gels, Porphyrins, Photopharmacology, Antimicrobial Phototoxicity

1. INTRODUCTION

Porphyrins have a relatively long history as photosensitizers and improvements in both the photoactive molecules and their incorporation into materials are currently being investigated for their potential applications in photocatalysis, wastewater treatment, and photodynamic therapy (PDT) [1-3]. It is remarkable to note that most clinically approved photosensitizers (PSs) for biomedical applications are porphyrins and their derivatives [4]. Research into porphyrins with different functional groups and central metal ions are currently being pursued to improve several features, such as the increased generation of singlet oxygen (SO), one type of reactive oxygen species (ROS). PDT typically requires three essential components, namely the photosensitizer (PS), light at a specific excitation wavelength, and molecular oxygen (MO) [5]. The core principle of PDT revolves around the generation of the excited state of the PS by

light of a specific wavelength that effectively promotes formation of the reactive form of the chromophore that transfers energy to the MO, which forms SO that in the most frequent applications can selectively damage bacterial or cells [6,7,8]. Thus, the efficient generation of SO from the PS is crucial for the successful application of PDT.

Microorganisms have played a substantial role in causing diseases in both humans and animals and are predicted to be a significant threat to civilization this century [9]. The daily use of antibiotics leads to their bacterial adaptation to negate toxicity, termed antimicrobial resistance (AMR), prompting a shift in focus within the scientific community from more classical active agents towards adopting PDT, known as antimicrobial PDT (aPDT), for treating infections [8,10]. The biggest advantages of this approach is that it can be used against both gram-positive and gram-negative bacteria [11,12] and in principle does not generate AMR, because ROS do not target specific sites. Staphylococcus aureus (*S. aureus*) is a gram-positive bacterium that typically resides within the human commensal microbiota, these organisms have the potential to induce infections that vary from minor skin issues and localized abscesses to severe conditions like osteomyelitis, endocarditis, and other illnesses [13,14,15]. Moreover, *S. aureus* has emerged as a notable cause of healthcare-associated infections (HAIs) [16,17]. Escherichia coli (*E. coli*) is a gram-negative bacterium which is multi-resistant to many antibiotics causing intestinal and bloodstream infections [18]. As bacteria increase their resistance to many antibiotics and become multi-drug resistant, currently available antibiotics are tending to be less effective than previously. To effectively treat bacterial infections, it is important to explore new materials or procedures as alternatives to antibiotics. Among various formulations, gels offer several advantages because of their thixotropic behaviour, higher retention time and excellent spreadability for topical administration [19,20].

Common limitations to the conversion of MO into SO are related to the high lipophilicity of the PS and their tendency to aggregate in solution. Alternatives have been designed either at the single molecular level, by modifying and tuning the photochemical properties of the PS or using nanostructured materials as carriers for their targeted use. Nanoparticle-based delivery systems, including polymeric nanoparticles, liposomes, and coordination polymer nanoparticles, have been widely explored for PS encapsulation to enhance solubility, stability, and therapeutic efficiency for PDT. However, the application of traditional nanocarriers for the noncovalent co-loading of drugs is often hampered due to several drawbacks, such as low co-loading efficiency (usually less than 10%), inadequate stability, and a significant risk of premature drug release during blood circulation [21]. These limitations often result in reduced

therapeutic efficacy and potential side effects, which hinder their clinical translation. In contrast, supramolecular gels have emerged as a promising alternative for excellent PS encapsulation and targeted delivery. Supramolecular gels form through the self-assembly of Low Molecular Weight Gelators (LMWGs) via non-covalent interactions like hydrogen bonding, π-π stacking, and hydrophobic interactions and a much less explored method for PS organization is the use of physical or supramolecular gels [22]. These gels are thermoreversible and rely on weak intermolecular forces rather than multivalency in polymeric systems. They also offer facile degradation, greater flexibility, and dynamic behaviour due to their shorter molecules and physical bonding [23]. From the best of our knowledge, there are very few studies that explored the use of supramolecular gels for aPDT. Fang et al. developed a spray hydrogel incorporating a supramolecular PS (methylene blue and closo-B12H12) for aPDT. This hydrogel exhibited around 99% aPDT efficacy against *S. aureus* and 95% against *E. coli* under 660 nm irradiation [24]. Zhang et al. developed an injectable supramolecular hydrogel based on fluorenyl methoxycarbonyl/berberine (Fmoc) incorporating C_{60}-PTC fullerenes for aPDT and achieved 100% aPDT efficacy against *S. aureus* under white light irradiation [25]. In the study by Xie et al., they formulated Fmoc-berberine encapsulated supramolecular gel which exhibited 36.9 % aPDT activity against *E. coli* and 100% against *S. aureus* under white light irradiation [26]. In this study, the formation of supramolecular gel is relatively easier to formulate, ensuring cost-effectiveness and potentially more scalable compared to the more complex spray hydrogel system. In the research done by Fmoc- C_{60}-PTC fullerenes system, they did not investigate drug release kinetics, whereas our study evaluates their release behaviour. Our gels have good encapsulation efficiency, improved mechanical stability, and prolonged PS retention (PS will not enter the surrounding environment during the treatment, hence no damage to the healthy cells and without the need for constant reapplication), leading to sustained therapeutic action. Their biocompatibility makes them versatile materials for various biomedical applications, including PDT.

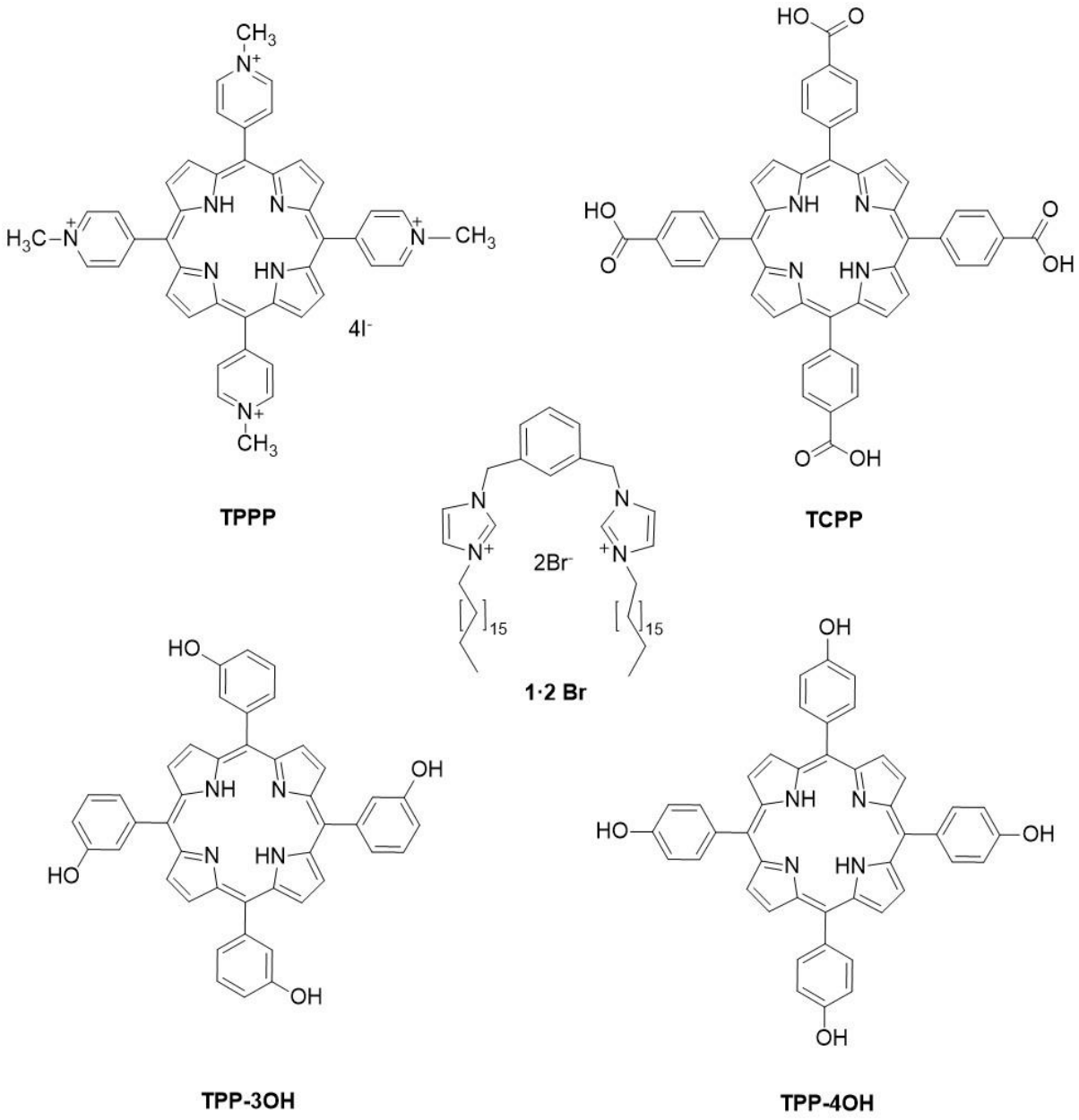

Figure 1. Molecular structures of the amphiphile 1·2 Br and the porphyrins (TCPP, TPPP, TPP-3OH, TPP-4OH) used in this study.

Supramolecular gels offer several advantages over conventional approaches, including their ability to address issues such as high lipophilicity and aggregation tendencies of the photosensitizer in solution. The surrounding environment of the chromophore within materials significantly influences the process, with the supramolecular structure having a great impact [27,28,29]. Our team has shown that incorporating 5,10,15,20-tetrakis(4-carboxylatephenyl)porphyrin (TCPPNa) [30] into a bis-imidazolium gelator matrix results in a 14-fold increase in singlet oxygen (SO) generation, while encapsulating PS Zinc(II)

phthalocyanine tetrasulfonic acid [31] within the same matrix enhances SO generation by 9-fold compared to their solution forms. Building on this finding, the four porphyrins—5,10,15,20-tetrakis(*N*-methyl-4-pyridinium)porphyrin tetraiodide (TPPP), 5,10,15,20-tetrakis(4-carboxyphenyl)porphyrin (TCPP), 5,10,15,20-tetrakis(3-hydroxyphenyl)porphyrin (TPP-3OH), and 5,10,15,20-tetrakis(4-hydroxyphenyl)porphyrin (TPP-4OH) which are structurally different—were selected to investigate how presence of different functional groups influence their incorporation into supramolecular gels. These porphyrins offer distinct chemical functionalities: TPPP introduces cationic charges, TCPP contains carboxyl groups, and TPP-3OH and TPP-4OH feature hydroxyl groups at the meta and para positions, respectively. TPP-3OH, a commercially available photosensitizer approved for clinical use in photodynamic therapy (PDT), was used as a reference in this study. This variation enables diverse non-covalent interactions, such as electrostatic attraction and hydrogen bonding, which can affect gel structure and stability and to ultimately define their interaction with the gelator. The selection was made to explore their impact on gel morphology, optical and mechanical properties, and singlet oxygen (SO) generation capabilities, extending our previous findings and paving the way for potential medical applications.

Consequently, we successfully performed aPDT experiments on *S. aureus* and *E. coli* to assess the efficacy of the prepared gels with photosensitizers in combating these bacteria.

2. EXPERIMENTAL PROCEDURES

2.1. Materials

This work's chemicals, reagents, and solvents are all analytical grades and were purchased commercially. Porphychem, France, supplied all the photosensitizers. Sigma-Aldrich provided the uric acid (UA). Phosphate Buffered Saline (PBS) was purchased from Loba chemicals. Milli-Q water (obtained with Millipore's Milli-Q Plus system) was used to prepare all samples. *E. coli* MTCC No. 40 and *S. aureus* MTCC No. 15029 Strain Ga2 was purchased from the Institute of Microbial Technology (IMTECH), India. Nutrient broth, nutrient agar and mannitol salt agar were purchased from Hi-media. The compound 1,3-bis[(3-octadecyl-1-imidazolio)methyl]benzene dibromide was made as previously described [32].

2.2. Gels Preparation

Gels containing 1·2 Br (12 mM) were prepared by mixing ethanol solutions of the gelator with Milli-Q water in a 1:1 ratio by volume. Since TPPP is water-soluble, a 2.5 mM stock solution

of TPPP was prepared in water, while the stock solutions of the other porphyrins TCPP (0.6 mM), TPP-3OH (2.5 mM), and TPP-4OH (2.5 mM) were prepared in ethanol. The appropriate volumes of each porphyrin solution were added to the gelator solution, ensuring compatibility with their respective solvents before combining with water in a 1:1 water-to-ethanol ratio for a total volume of 1 mL gel. The final concentration of the porphyrin in the gel is 0.3 mM. After gentle mixing of all components, the solution vials were sealed and allowed to stand undisturbed at room temperature (approximately 25 °C). When no flow was seen while inverting the vial, gels were assumed to have formed.

2.3. Singlet Oxygen Production

Uric Acid (UA) was employed as a chemical trapping agent. The production of SO was measured by monitoring the decrease in absorbance of UA. A 10 mm cuvette holding the sample was irradiated for 30 minutes, with absorption spectra collected every 5 minutes in the wavelength range of 200-400 nm using a LABINDIA Ultraviolet 3200 spectrometer. The cuvette containing the sample was irradiated using a λ = 650 nm laser (diode module with 50 mW power, operating voltage 5V DC and operating current 500 mA).

For irradiation experiments, an aliquot of 0.2 mL containing either the photosensitizer in a 1:1 water : ethanol mixture or a gel with porphyrin prepared with the same solvent composition was added to 1.8 mL of a 0.1 mM UA solution in 2 mM PBS, resulting in a final porphyrin concentration of 10 µM and a final ethanol content of 5%. For this, a 0.6 mM UA stock solution was prepared in water. A 100 mM PBS stock solution was also prepared in water.

2.4.Gel Characterization

Each gel's rheology was studied using a Haake Rheostress 1 rheometer (Thermo Fisher Scientific, Karlsruhe, Germany) linked to a Thermo Haake Phoenix II + Haake C25P temperature controller and fitted with parallel plate geometry (Haake PP35 L Ti, 35 mm diameter, 1 mm gap between plates). All measurements were taken at a temperature of 298.15 K. Each gel, either with or without porphyrin, was prepared on a 5.1 cm diameter plastic petri plates with a parafilm cover, yielding a total volume of 3.6 ml. They were carefully sealed, maintained at room temperature for two days, and used for analysis. Gels were carefully transferred to the rheometer plate by inverting the parafilm to avoid breakage, and the excess part was removed to match the plate geometry. During the assessment of oscillation amplitude

tests at a deformation frequency of n=1 Hz, the ability to resist deformation and rupture were evaluated.

Scanning electron microscope (SEM) images were acquired using HITACHI SU8010 FE-SEM system at SAIF/CIL, Panjab University, India. A round borosilicate glass slide containing gel sample was placed on top of the aluminium stub using double sided adhesive carbon tape. Then, gel containing stubs was placed under gold sputter coating machine for 20 sec at 15 mA and images were captured at accelerating voltage of 10 kV.

UV-Visible absorption spectroscopy was performed using a Shimadzu UV-1800 UV-Vis spectrophotometer. Fluorescence spectroscopy was measured using an SLM Aminco 8100 spectrofluorimeter. All measurements were carried out using quartz cuvettes with 10 mm path length.

2.5. Release Studies

Amber glass Franz-type diffusion cells (FDC 400, Crown Glass Co., Somerville, NY, USA) with a 0.64 cm^2 diffusion area were utilized for the release studies of gels containing all porphyrins. These cells were mounted into a Microette system (Hanson Research, Chatsworth, CA, USA) equipped with six Franz cells, alongside a Tamson T1000 thermostat bath [33]. Dialysis membranes (Thermoscientific dialysis membrane, MWCO 10,000 Da, USA), pre-hydrated in a 7:3 ethanol:water solution, were positioned within the Franz-type diffusion cells. The receptor chamber was filled with a DMSO:H_2O (1:9) solution, maintaining SINK conditions. The dialysis membrane and the donor container were placed onto the glass receptor chamber and secured with a joint. The Franz-type cells were connected to a temperature-controlled circulating bath set at 32 ^oC ± 0.5 ^oC. Gels were placed into the donor compartment on top of the dialysis membranes, with the donor compartment sealed using paraffin film to limit solvent evaporation. Samples were collected at specified time intervals, with each sample withdrawn being replaced by an equal volume of the receptor solution. All release experiments were done in triplicate and the whole parameters are summarised in Table S1.

Analytical Procedures for Release Studies

All porphyrin solutions were prepared using DMSO:H_2O (1:9) as the solvent and their calibration curves (Figure S1) were made in the range of 0.13-4.21 μM (TPPP), 0.20-1.25 μM (TCPP) and 0.0022-0.15 μM (TPP-3OH & TPP-4OH). These calibration curves were analysed

by performing a linear regression (TPPP & TCPP) and non-linear regression one-phase association (TPP-3OH & TPP-4OH) method using GraphPad Prism® (version 5.00, GraphPad software, Inc., USA). The emission of the sample solutions at λ_{ex} = 417 nm was determined using SLM Aminco 8100 spectrofluorimeter with a xenon lamp and thermostatic cuvette holder. Subsequently, the emission values of the sample solutions were fitted into the corresponding calibration curve to determine the concentration of the samples.

2.6. Antibacterial Studies

The aPDT activity of each of the photosensitizers, both in solution and in the gel, was evaluated by the colony forming unit (CFU) method [34] against gram negative bacteria *E. coli* and gram-positive bacteria *S. aureus*. All materials used for experiments were sterilized. The experiment was performed into the following groups: control (bacterial cells without dose), phototoxicity (bacterial cells irradiated with PS, PS@Gel), dark toxicity (bacterial cells incubated with gel, PS@Gel in dark). Nutrient broth solution was prepared for the bacterial growth. A single colony was taken from the bacterial culture plate and inoculated in the above prepared nutrient broth solution and was kept at 37 °C for 24 h. First, 150 µL of freshly prepared bacterial suspension was added into each Eppendorf tube containing 50 µL of the 12 mM gel with each porphyrin at a concentration of 25 µM, no incubation time is given. The samples were then irradiated with laser light of λ = 650 nm (50 mW power, operating voltage 5V DC, operating current 500 mA, Irradiance 63.69 mW/cm^2, Fluence 114.64 J/cm^2) for 30 mins. The gel was composed of ethanol and water in a 1:1 ratio by volume, with this ethanol-to-water solution used as a control. Following irradiation, the samples were serially diluted with a dilution factor of 10^3 for *E. coli* and 10^6 for *S. aureus*. Then 100 µl of the dilution was taken and plated onto nutrient agar plates (for *E. coli*) and mannitol salt agar plates (for *S. aureus*). Bacterial load (CFU/mL) of the inoculum before the treatment of *E. coli* and *S. aureus* is given in the Table S2. After incubation of these plates for 24h at 37 ºC, colonies were counted to determine CFUs. Each experiment was performed in triplicate. Bacterial suspension without any sample was used as a control.

3. RESULTS AND DISCUSSION

3.1. Self-assembly of the gels

The gemini imidazolium-based amphiphile 1·2Br (Figure 1) serves as our molecular gelator, inducing the formation of supramolecular gels through self-assembly in water-ethanol mixtures. With excellent solubility in ethanol, the introduction of water, acting as an anti-

solvent, initiates the self-assembly process and facilitates fibre formation [35]. The formation of the gel occurs upon adding water to an ethanolic solution containing 1·2 Br, resulting in a final concentration of 12 mM amphiphile with a water to ethanol ratio of 1 to 1 by volume (Figure 2).

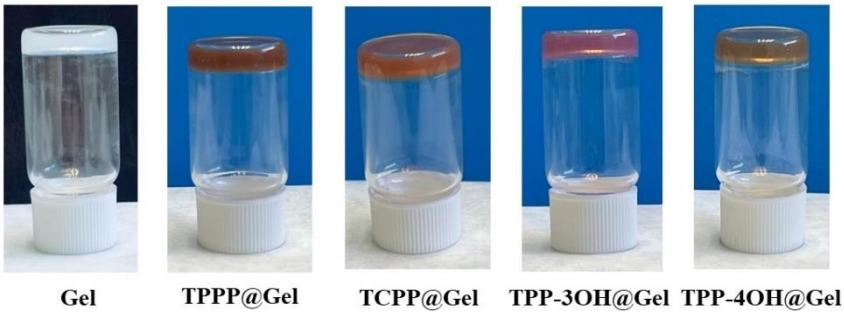

Figure 2. Gels of 1·2 Br at a concentration of 12 mM in a 1:1 water-ethanol ratio, both without porphyrin and with a porphyrin concentration of 0.3 mM for TPPP, TCPP, TPP-3OH, and TPP-4OH.

The prepared gels demonstrated resilience to movement and remained stable for several months when stored at room temperature (approximately 25 °C). In the release experiments of all porphyrin gels, TCPP showed a minimal release percentage of 0.06%, while the other porphyrins exhibited even lower release percentages, below 0.02% (Figure S1E). In the release experiments of all porphyrin gels, TCPP showed a minimal release percentage of 0.06%, while the other porphyrins exhibited even lower release percentages, below 0.02% (Figure S1E). This result demonstrates that drug release from the gel is negligible in all cases under the conditions studied, indicating effective retention of the porphyrins within the gel matrix. It suggests that the quantity of porphyrins used in gel preparation is completely incorporated into the fibers rather than residing in the interstitial liquid between them. This finding is in line with our previous studies, the XRD findings confirm the incorporation of porphyrin into the fibers rather than its presence in interstitial spaces. This is evident from the significant changes in diffraction patterns with varying TCPP concentrations, indicating that porphyrin loading influences the overall fiber structure. If porphyrins were only in the interstitial liquid, their impact on the XRD patterns would be minimal [30]. This observation is consistent with findings from our subsequent research, where dynamic experiments demonstrated that TCPPNa porphyrin was integrated into the gel fibers rather than residing in the interstitial fluid. Real-time tracking using TIRF microscopy revealed the movement of TCPPNa along the fibers upon irradiation, further supporting the idea that the porphyrin migrates along the fibers. This behaviour

underscores the conclusion that the porphyrins are firmly incorporated into the gel matrix, rather than diffusing freely in the surrounding solvent [36].

Rheological analysis was used to determine the mechanical characteristics of the porphyrin gels. Table 1 presents the viscoelastic parameters that were derived from the stress sweep experiments. Shear-Stress profiles of the gel and after the incorporation of the each of the four porphyrins are shown in Figure 3. The G' (storage moduli) is over the G'' (loss moduli) in all the samples which shows the elastic response of these gels [23] and wide linear visco-elastic regions are observed. When comparing the gel without any porphyrin, the gels with porphyrins has higher values of G' and G''. This effect indicates that the presence of porphyrin molecules in the gel matrix increases its resistance to deformation under applied stress. Gel without any porphyrin showed a critical stress value (CSV) of 63 Pa (Figure 3A). TPPP facilitates ionic interactions with the counter anions of 1·2 Br, helping to partially stabilize the gel structure and increasing the critical stress value from 63 to 87 Pa (Figure 3B). However, since TPPP is cationic and highly soluble in water, its presence in the aqueous phase can enhance overall ionic interactions within the gel. Nevertheless, the electrostatic repulsion between the cationic TPPP and the cationic gelator may limit the effectiveness of these interactions, ultimately resulting in a gel that, while stronger than the plain gel, still exhibits lower mechanical strength than the other porphyrin gels. TCPP gel (Figure 3C), with a CSV of 145 Pa, benefits significantly from the presence of carboxyl groups in TCPP, which can form multiple hydrogen bonds and electrostatic interactions between the porphyrin and the gelator. This enhances the cohesion and rigidity of the gel structure, leading to improved mechanical strength.

Table 1. Storage modulus (G′), loss modulus (G′′), and critical stress of gels obtained from stress sweep experiments as function of porphyrin gels loading at 25 ºC.

Sample	G' (Pa) [a]	G''(Pa) [a]	Critical Stress (Pa) [b]
A: Gel without porphyrin	5837	1068	63
B: TPPP@Gel [c]	9912	1818	87
C: TCPP@Gel [c]	20911	4295	145
D: TPP-3OH@Gel [c]	22342	6811	107
E: TPP-4OH@Gel [c]	93942	15020	355

[a] Values at the linear viscoelastic regime. [b] The critical stress value is defined as a noticeable change in storage and loss moduli. [c] Concentration of porphyrin is 0.3 mM.

TPP-3OH gel (Figure 3D) has a higher CSV value of 107 Pa because the hydroxyl groups in the 3-position of the phenyl ring allow hydrogen bonding and spatial arrangement within the gel, resulting in suboptimal network integrity because of possible conformational variety. TPP-4OH' gel (Figure 3E) had the highest CSV value of 355 Pa. The 4-position of the hydroxyl groups on the phenyl ring may allow the most effective and directional hydrogen bonding with the gel network, significantly enhancing the structural stability and mechanical strength. This optimal interaction leads to a gel structure that can withstand greater applied stress, illustrating the critical role of functional group positioning in determining the mechanical properties of the porphyrin-containing gels. A similar rheological behaviour was observed with the incorporation of TCPPNa into the same supramolecular gel studied earlier by our group [30]. The higher CSV values of the porphyrin-containing gels suggest that the porphyrins are contributing to the strengthening of the gel network established during the self-assembly process.

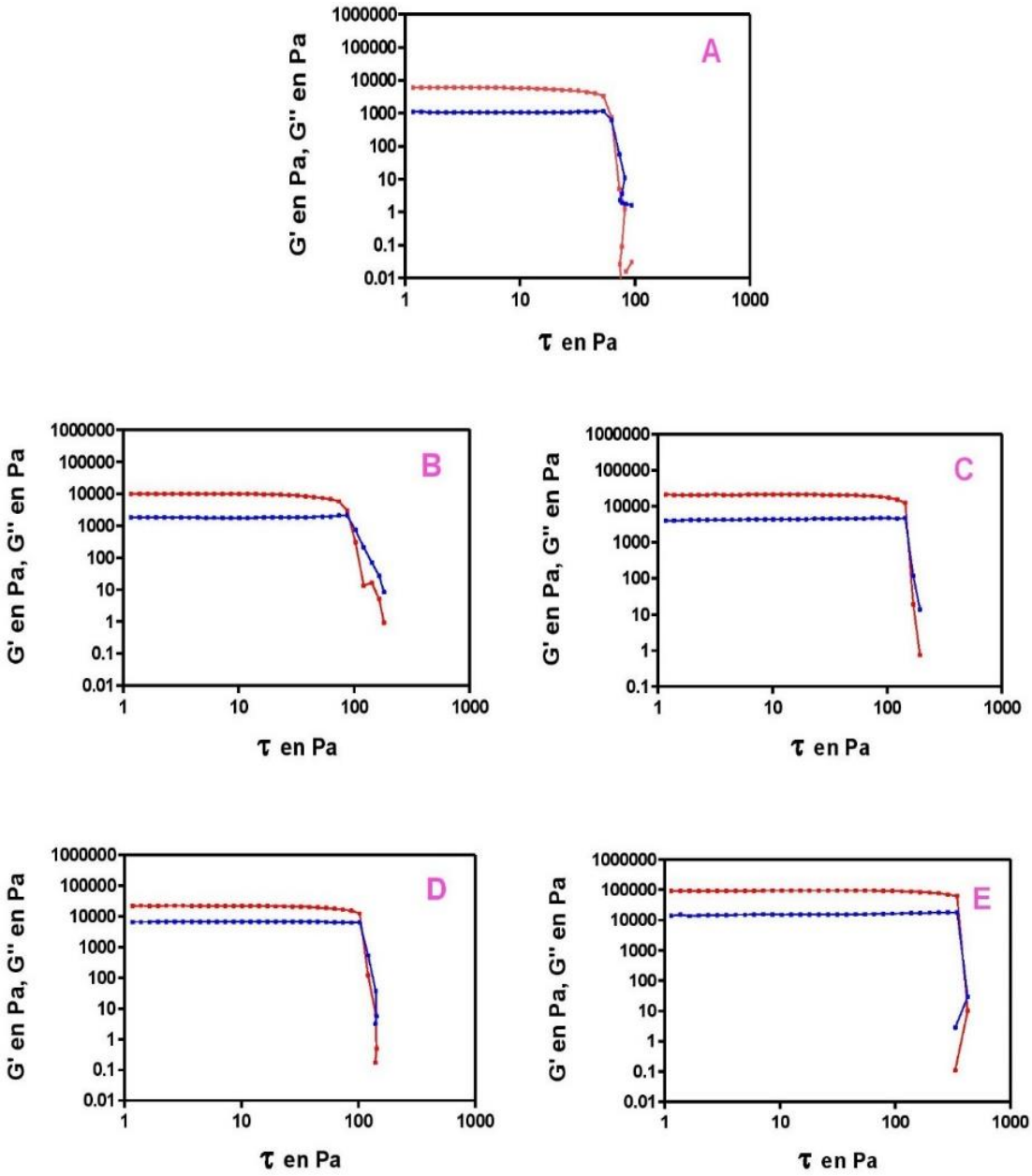

Figure 3. Shear Stress profiles showing storage (G', red curve) and loss (G'', blue curve) moduli from gels of 1.2Br at 12 mM in water-ethanol ratio 1:1 without porphyrin (A) and with a porphyrin concentration of 0.3 mM of TPPP (B), TCPP (C), TPP-3OH (D) and TPP-4OH (E).

3.2. Structure and Morphology

The SEM micrographs (Figure 4) of the xerogels show that, in the absence of any photosensitizer, the xerogel exhibits a morphology characterized by well-defined micrometric-long fibres spanning a width range from 50 to 220 nm. This initial observation established a baseline understanding of the gel's morphology. The histograms indicate that both the plain gel and after the incorporation of each of the four porphyrins consistently exhibit fibres with widths ranging from 50 to 200 nm. This shared characteristic underscores a fundamental aspect of gel

morphology unaffected by the presence of different porphyrins. The average fiber width of the 1.2 Br gel is 94 nm, with 14 fibers observed, indicating that thicker fibers are less abundant in this system. In comparison, the porphyrin gels exhibit slightly smaller fiber widths but with more abundant fibers. TPPP has an average fiber width of 87 nm with 19 fibers, and TPP-3OH shows a similar width of 87 nm but with 24 fibers. TCPP and TPP-4OH have average fiber widths of 80 nm and 79 nm, respectively, with the highest fiber counts observed: 28 for TCPP and 25 for TPP-4OH. While the 1.2 Br system has the thickest fibers but the fewest in number, the porphyrin gels show a trend of smaller fiber widths and higher quantities of fibers, suggesting that the inclusion of porphyrins leads to a higher density of thinner fibers compared to 1.2 Br. Additionally, the 1.2 Br gel exhibits a less uniform distribution of fiber widths, with a wider variation in size, whereas the porphyrin gels show a more consistent and narrower range of fiber widths.

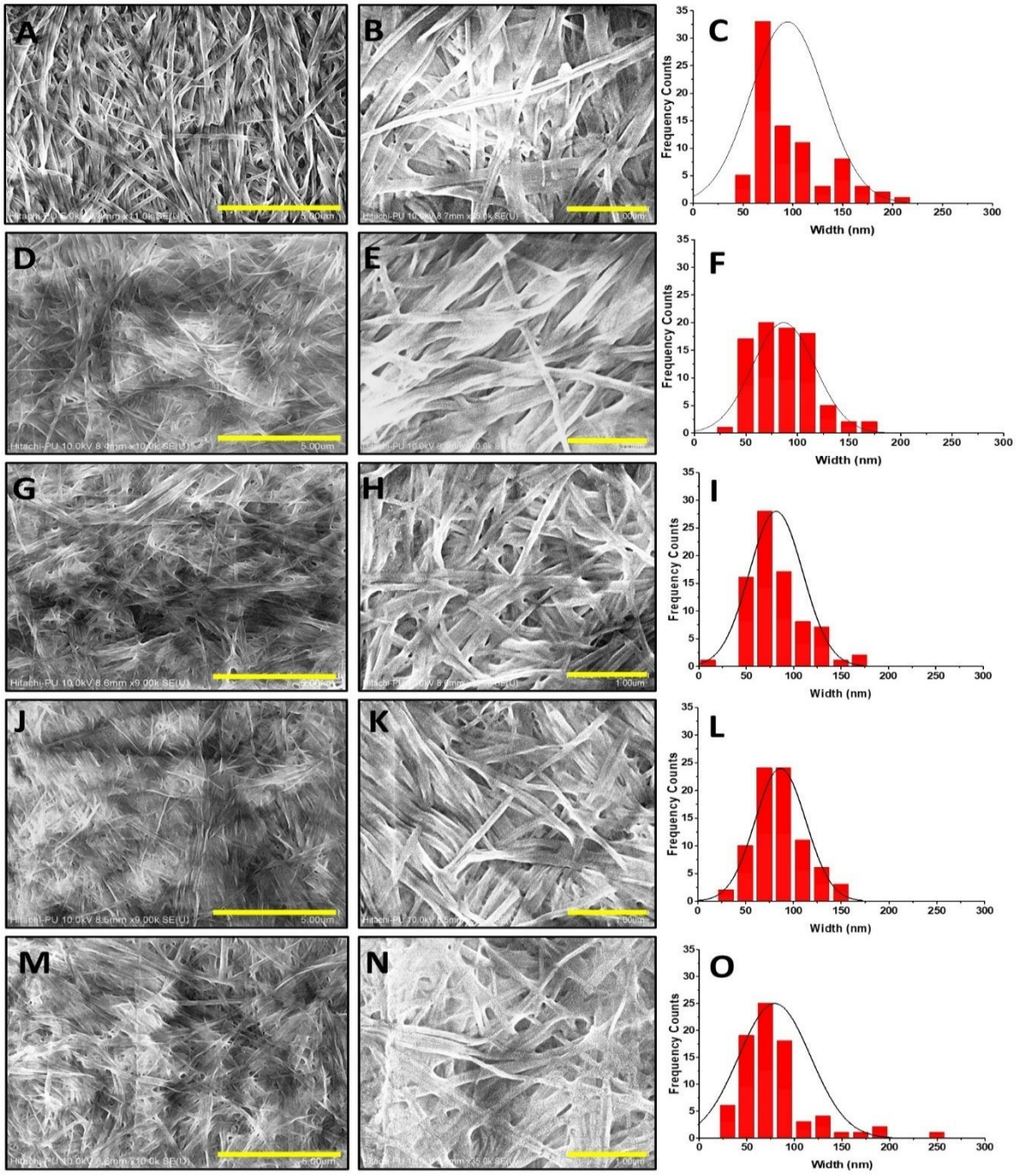

Figure 4. SEM images of xerogels prepared from gels at a 12 mM concentration of 1·2Br: without any porphyrin (Images A and B), with TPPP (Images D and E), with TCPP (Images G and H), with TPP-3OH (Images J and K), and with TPP-4OH (Images M and O). The corresponding fiber width distribution histograms are shown in C (for the sample without porphyrin), F (for TPPP), I (for TCPP), L (for TPP-3OH), and N (for TPP-4OH). The scale bars in the micrographs represent 5 μm in the left column and 1 μm in the right column. The porphyrin concentration in all the gels is 25 μM.

3.3. Photophysical properties and SO generation

Figures 5A and B show the absorption spectra of each of all four porphyrins (10 µM) in solvent ratio water-ethanol 1:1 (solution) and in gel respectively. They display the typical features of this class of molecules, with their Soret band and Q bands listed in Table 2, except TPPP. TPPP@Sol lacks the Q2 band in its absorption spectrum. The absorption spectra of all gels with photosensitizers showed an increase in the baseline because of the light scattered by the fibrillar network of the gel, together with a moderate bathochromic shift 3-7 nm, except TPPP. TPPP@Gel do not have the Q2, Q3, and Q4 bands in its absorption spectrum. Its cationic nature likely leads to electrostatic repulsion with the cationic gelator. This repulsion may limit interactions between TPPP and the gel, thereby preventing the typical electronic transitions associated with these bands, which are typically related to the excited state transitions within the porphyrin ring system. This is also associated with the broad and intense emission peaks observed in TPPP@Gel, which can be attributed to the aggregation of TPPP within the gel matrix. This aggregation may lead to self-quenching in the broadening of the emission peaks.

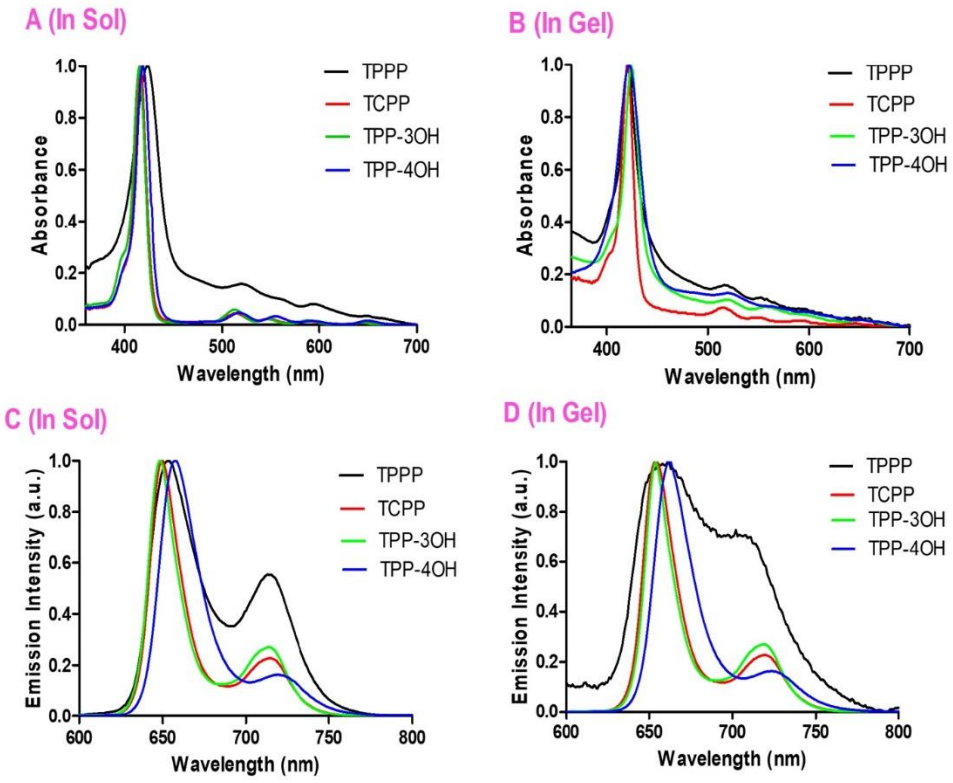

Figure 5. Normalized absorption spectra (A – in solution, B – in gel) and fluorescence emission spectra (C - in solution, D – in gel) of all porphyrins. The solution and gel both have the same solvent ratio of water to ethanol (1:1) and the same porphyrin concentration. Experimental conditions: Porphyrin = 10 µM, 1·2Br = 12 mM.

Table 2. Absorption bands (Soret band and Q-bands) of each of the porphyrins in solution and in gel.

Porphyrin		Wavelength (nm)				
		Soret band	Q1 band	Q2 band	Q3 band	Q4 band
TPPP	[a]	423	519	[c]	593	649
	[b]	422	519	[c]	[c]	[c]
TCPP	[a]	416	513	548	589	645
	[b]	422	518	548	588	652
TPP-3OH	[a]	415	512	547	588	644
	[b]	421	515	548	583	546
TPP-4OH	[a]	418	517	554	593	650
	[b]	424	520	562	586	656

[a] Porphyrin in solution. [b] Porphyrin in gel. [c] Q-Band is not observed.

The emission spectra of porphyrins in a water-ethanol mixture (1:1) is characterised by the presence of two distinct bands λ_a = 650 nm and λ_b = 714 nm (Figure 5C). Like for the absorption spectra, a modest bathochromic shift (4-6 nm) is observed in the emission spectra when the photosensitizers are incorporated into the gel (Figure 5D), indicative of reduced aggregation. This behaviour aligns with previously reported observations of TCPP in polar solvent environments, where reduced aggregation is noted due to the presence of ethanol, a feature that is maintained upon incorporation into gels by our group [30]. Figures 5C and D show the emission spectra of each of the porphyrins in sol and in gel, with their bands listed in Table 3.

Table 3. Emission bands of each of the porphyrins in solution and in gel with 1·2 Br.

Porphyrin		Wavelength (nm)	
		First Band (λ_a)	Second Band (λ_b)
TPPP	[a]	654	715
	[b]	661	702
TCPP	[a]	650	714
	[b]	646	712
TPP-3OH	[a]	648	713
	[b]	665	[c]
TPP-4OH	[a]	658	719
	[b]	665	[c]

[a] Porphyrin in solution. [b] Porphyrin in gel. [c] Band is not observed.

The ability of each photosensitizer to generate SO in both solution and gel was evaluated using UA as a molecular probe by irradiating with λ = 650 nm laser for 30 minutes. Uric acid (UA) was employed as a chemical trapping agent that undergoes oxidation to form parabanic acid [37] by reaction with SO, resulting in a spectrometrically measurable decrease in the

absorbance region associated with the probe [38]. Control studies with UA and no porphyrin in solution showed minimal degradation of 6 % whereas in the presence of the plain gel UA showed the decrease of around 28% after 30 minutes of irradiation. The 28% degradation of UA observed in the gel without any porphyrin could be due to minor interactions between the gel matrix and the light during irradiation. While the gel does not contain a photosensitizer, its fibrillar network may facilitate some low-level photochemical activity, leading to the degradation of UA. Incorporating TPP-4OH into the gel caused a significant decrease in uric acid absorption, reducing it by up to 74%, compared to just a 5% reduction when TPP-4OH was in solution. TCPP exhibited the most substantial effect, with a 93% reduction in uric acid absorption when incorporated into the gel, while only a 69% reduction was observed in solution. Figure 6 illustrates these results and demonstrates that the encapsulation of porphyrin within the gel significantly enhances its SO generation ability. The same studies were conducted on the other porphyrins, evaluating their ability to generate singlet oxygen in both solution and gel forms (Figure S2). Absorption spectra of UA after addition of each of the porphyrin in solution and in 1·2 Br gel followed by 30 minutes irradiation is shown in Figure S3.

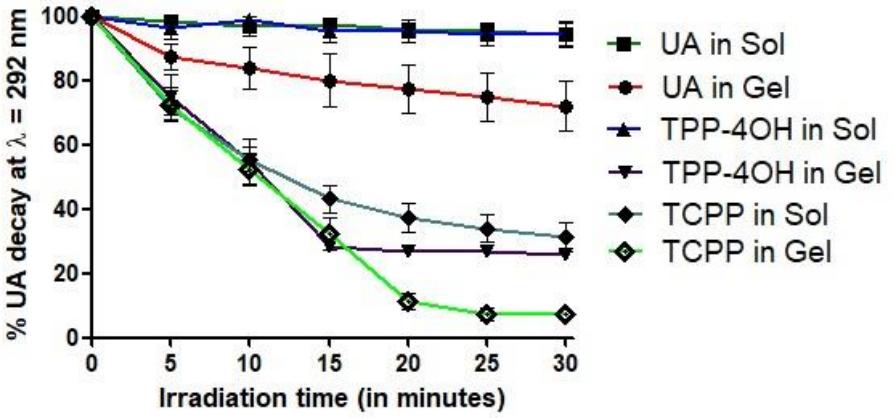

Figure 6. Percentage decrease of UA absorption recorded upon irradiation of UA, TPP-4OH and TCPP both in solution and after incorporation into the gel.

3.4. Antibacterial Studies

To evaluate the antimicrobial photodynamic therapy (aPDT) efficacy of the porphyrin-containing gels, the CFU method was employed to assess the results for *E. coli* after irradiation with a λ = 650 nm laser for 30 minutes. For *E. coli*, both dark as well as light toxicity experiments were performed on all the porphyrin gels. Under both dark and light conditions, the gel demonstrated a 40% reduction in CFU count for *E. coli* and *S. aureus* (Figure S4),

indicating that light had no effect on the gel. The reduction in CFU can be partly attributed to electrostatic interactions between the cationic gelator and the negatively charged bacterial membrane [39], which may disrupt the membrane and contribute to bactericidal activity even without light. As the gel is composed of ethanol and water in a 1:1 ratio, this solvent system was used as a control. For *E. coli*, water to ethanol 1:1 ratio solvent system with and without porphyrin exhibited a 70% reduction in CFU count (Figure 7B) (bacterial images – 7C), while the gel demonstrated a 40% reduction.

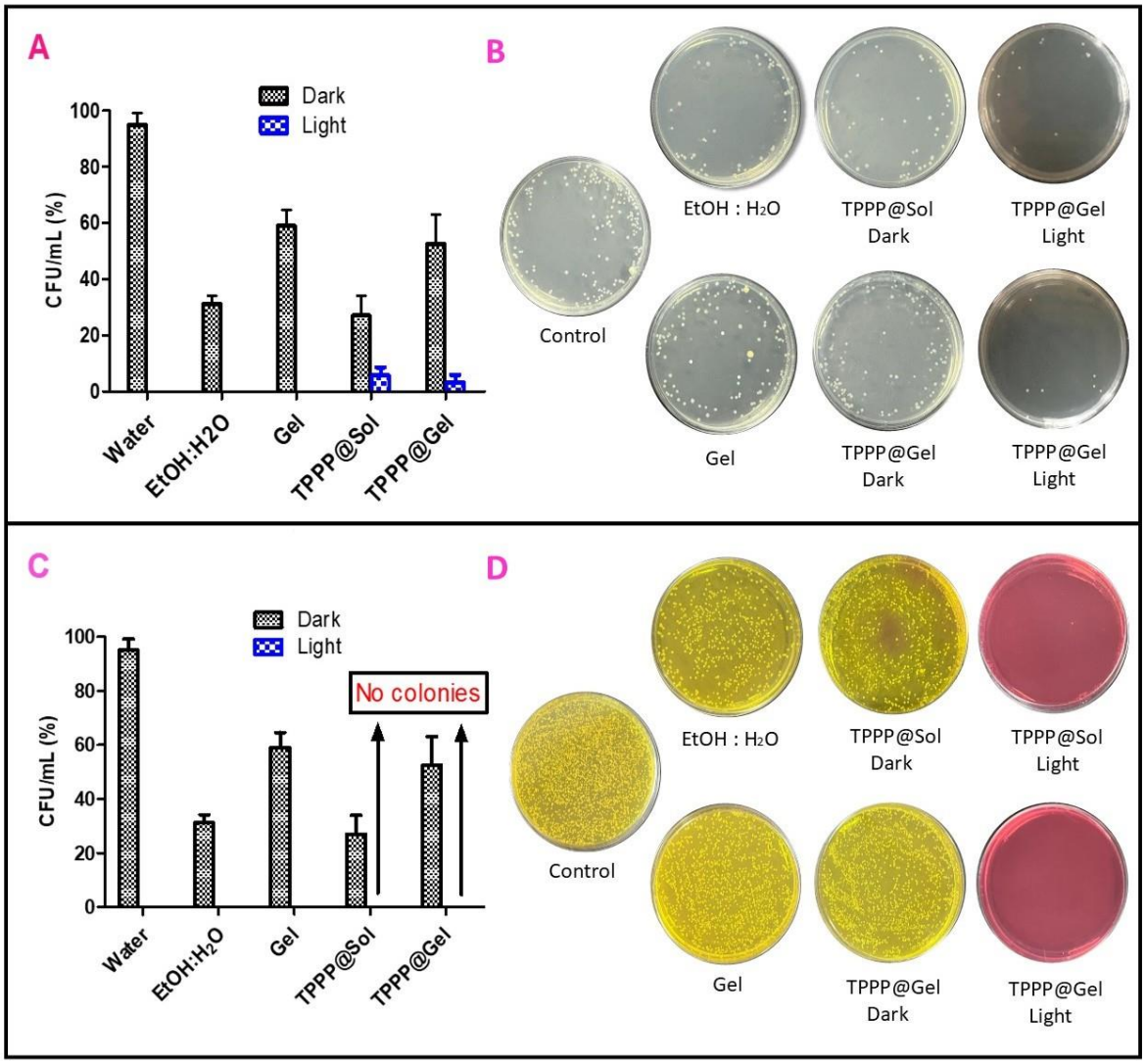

Figure 7. Graphs showing CFU/mL (%) for *E. coli* (A) TPPP (colony images–B), and for *S. aureus* (C) TPPP (colony images–D). The porphyrin concentration in all the gels is 25 µM.

Ethanol itself is a well-known antimicrobial agent [40], which explains the 70% bacterial killing observed in the solvent system. However, when incorporated into the gel, the ethanol is

more restricted due to its confinement within the gel matrix. This limitation reduces the free movement of ethanol and consequently its ability to effectively interact with bacterial membranes, leading to a lower bactericidal activity. Specifically, under light conditions, TPPP@Gel exhibited the highest 97% reduction in CFU count against *E. coli* more than the gel without porphyrin (Figure 7A) (bacterial images – 7B). TPPP@Sol showed 94% CFU reduction under the same conditions against *E. coli*. Similar studies were conducted on the other porphyrins in both solution and gel forms (Figure S5).

Following this, the experiments targeting *S. aureus* were performed only using TPPP because it showed the highest CFU reduction count against *E. coli* and *S. aureus* bacteria have negatively charged teichoic acids in their thick peptidoglycan layer [41]. Since both TPPP and 1·2 Br gelator are cationic, it is expected to bind more to *S. aureus* cells and inhibit them more. Under light conditions, TPPP@Gel showed complete reduction in CFU count within 30 mins of irradiation for *S. aureus*, more than the gel without porphyrin (Figure 7C) (bacterial images – 7D) (colony images - Figure 7D). This same behaviour was also observed with TPPP@Sol under the same conditions against *S. aureus*. The main advantage of the gel system over the solvent system provides a stable platform for the porphyrins, ensuring their local concentration at the site of application. This not only enhances the antimicrobial effect but also allows for a more sustained exposure to the photosensitizer without the need for constant reapplication, unlike the solvent system which tend to dissipate more quickly.

It is widely recognized that a 3-log (99.9%) reduction in bacterial load is the standard threshold for evaluating the efficacy of antimicrobial activity [42]. While the formulations tested in this study did not meet the 99.9% reduction threshold for *E. coli*, it is noteworthy that it is successfully achieved for *Staphylococcus aureus* (S. aureus). This finding underscores the potential effectiveness of the supramolecular gel-based formulations for certain bacterial strains. The primary objective of this study was to assess the potential of these formulations in the context of aPDT). Although the reduction observed in *E. coli* did not meet the 99.9% reduction of bacterial load, the substantial antimicrobial effect demonstrated against *S. aureus* highlights the potential of these gel-based systems. These findings lay a solid foundation for further optimization, aiming to improve the formulations' antimicrobial efficacy and extend their activity to a wider range of bacterial pathogens. From the results, it is evident that aPDT was very effective when the porphyrin is incorporated into the gel, and the killing of bacteria was observed within 30 minutes of irradiation. CFU reduction (%) after 30 minutes of irradiation for both *E. coli* and *S. aureus* with each photosensitizer both in solution and in gel forms is presented in Table S3.

4. CONCLUSION

The supramolecular gels discussed exhibit significant potential across various applications resulting from its enhanced SO generation upon light exposure. The improved properties compared to solution are attributed to the non-covalent interactions between the porphyrins and the gelator within the supramolecular system. Notably, the gel and gels after the incorporation of different porphyrins had similar morphology. Rheological studies reveal that incorporating porphyrins substantially affects gel mechanical properties, with TPPP moderately enhancing gel strength despite ionic repulsion, while TCPP substantially improves strength through strong hydrogen bonding and electrostatic interactions facilitated by its carboxyl groups. The positioning of hydroxyl groups on porphyrins significantly impacts the mechanical properties of the gels, with TPP-4OH demonstrating good structural stability and mechanical strength presumably resulting from hydrogen bonding interactions. The incorporation of porphyrins into the gel significantly enhances their ability to generate SO as evidenced by the greater reduction in UA absorption in the gel compared to the solution. This highlights the role of the gel matrix in improving the photosensitizers photodynamic efficiency. Additionally, the aPDT experiments demonstrate that supramolecular gels when incorporated with porphyrins are effective against both gram-negative and gram-positive bacteria, with TPPP@Gel exhibiting the highest antimicrobial activity within 30 minutes of irradiation. The ability of these composite gels to effectively generate SO and exhibit antimicrobial properties underscores their potential for diverse biomedical applications, including wound healing. These findings highlight the importance of porphyrin structure and non-covalent interactions in creating strong, multifunctional nanomaterials, representing a significant advancement in the development of aPDT.

5. ACKNOWLEDGEMENTS

We thank Project PID-2023-146658NB-C32 funded by MICIU/AEI /10.13039/501100011033 and by FEDER, UE. AGAUR (Generalitat de Catalunya) for a grant to consolidated research groups 2021 SGR 01085. K.A. and S. B. thank Generalitat de Catalunya for predoctoral FI and FI-SDUR scholarships. The authors also thank Sophisticated Analytical Instrumental Facility (SAIF) and Central Instrumentation Laboratory (CIL) at Panjab University, India.

6. REFERENCES

(1) Zakavi, S.; Nazari, N.; Sardivand-Chegini, I.; Qodrati-Nasrabadi, F. A Porphyrin Derivative with Highly Red Shifted and Intensified Absorption Bands Immobilized into the Mesopores of Nanostructured Amberlite: Synthesis, Characterization and Photocatalytic Activity. *J. Photochem. Photobiol. A Chem.* **2023**, *442*, 114751. https://doi.org/10.1016/j.jphotochem.2023.114751.

(2) Savelyeva, I. O.; Zhdanova, K. A.; Gradova, M. A.; Gradov, O. V; Bragina, N. A. Cationic Porphyrins as Antimicrobial and Antiviral Agents in Photodynamic Therapy. *Current Issues in Molecular Biology*. **2023**, 12, 9793–9822. https://doi.org/10.3390/cimb45120612.

(3) Zhang, Y.; Ren, K.; Wang, L.; Wang, L.; Fan, Z. Porphyrin-Based Heterogeneous Photocatalysts for Solar Energy Conversion. *Chinese Chem. Lett.* **2022**, *33*, 33–60. https://doi.org/10.1016/j.cclet.2021.06.013.

(4) Garcia-Sampedro, A.; Tabero, A.; Mahamed, I.; Acedo, P. Multimodal Use of the Porphyrin TMPyP: From Cancer Therapy to Antimicrobial Applications. *J. Porphyr. Phthalocyanines.* **2019**, *23*, 11–27. https://doi.org/10.1142/S1088424619500111.

(5) Tavakkoli Yaraki, M.; Liu, B.; Tan, Y. N. *Emerging Strategies in Enhancing Singlet Oxygen Generation of Nano-Photosensitizers Toward Advanced Phototherapy*. *Nanomicro letters*. **2022**, 14, 123. https://doi.org/10.1007/s40820-022-00856-y.

(6) Di Mascio, P.; Martinez, G. R.; Miyamoto, S.; Ronsein, G. E.; Medeiros, M. H. G.; Cadet, J. Singlet Molecular Oxygen Reactions with Nucleic Acids, Lipids, and Proteins. *Chem. Rev.* **2019**, *119*, 2043–2086. https://doi.org/10.1021/acs.chemrev.8b00554.

(7) Chen, J.; Fan, T.; Xie, Z.; Zeng, Q.; Xue, P.; Zheng, T.; Chen, Y.; Luo, X.; Zhang, H. Advances in Nanomaterials for Photodynamic Therapy Applications: Status and Challenges. *Biomaterials.* **2020**, *237*, 119827. https://doi.org/10.1016/j.biomaterials.2020.119827.

(8) Sharma, B.; Thakur, V.; Kaur, G.; Chaudhary, G. R. Efficient Photodynamic Therapy against Gram-Positive and Gram-Negative Bacteria Using Rose Bengal Encapsulated in Metallocatanionic Vesicles in the Presence of Visible Light. *ACS Appl. Bio Mater.* **2020**, *3*, 8515–8524. https://doi.org/10.1021/acsabm.0c00901.

(9) Kumar, R.; Sood, U.; Kaur, J.; Anand, S.; Gupta, V.; Patil, K. S.; Lal, R. The Rising Dominance of Microbiology: What to Expect in the next 15 Years? *Microb. Biotechnol.* **2022**, *15*, 110–128. https://doi.org/10.1111/1751-7915.13953.

(10) Klausen, M.; Ucuncu, M.; Bradley, M. Design of Photosensitizing Agents for Targeted Antimicrobial Photodynamic Therapy. *Molecules* **2020**, *25*, 5239. https://doi.org/10.3390/molecules25225239.

(11) Jia, H.-R.; Zhu, Y.-X.; Chen, Z.; Wu, F.-G. Cholesterol-Assisted Bacterial Cell Surface Engineering for Photodynamic Inactivation of Gram-Positive and Gram-Negative Bacteria. *ACS Appl. Mater. Interfaces* **2017**, *9*, 15943–15951. https://doi.org/10.1021/acsami.7b02562.

(12) Yang, X.; Xia, P.; Zhang, Y.; Lian, S.; Li, H.; Zhu, G.; Wang, P. Photothermal Nano-Antibiotic for Effective Treatment of Multidrug-Resistant Bacterial Infection. *ACS Appl. Bio Mater.* **2020**, *3*, 5395–5406. https://doi.org/10.1021/acsabm.0c00702.

(13) Kim, C.-J.; Song, K.-H.; Choe, P. G.; Park, W. B.; Kim, E. S.; Park, K. U.; Kim, N. J.; Park, K.-H.; Kwak, Y. G.; Cheon, S.; Jang, H.-C.; Kim, Y. K.; Lee, S. H.; Kiem, S.-M.; Lee, S.; Kim, H. Bin; Oh, M. The Microbiological Characteristics of Staphylococcus Aureus Isolated from Patients with Native Valve Infective Endocarditis. *Virulence* **2019**, *10*, 948–956. https://doi.org/10.1080/21505594.2019.1685631.

(14) Urish, K. L; Cassat, J.E. Staphylococcus Aureus Osteomyelitis: Bone, Bugs, and

Surgery. *Infect. Immun.* **2020**, *88*. https://doi.org/10.1128/iai.00932-19.
(15) Becker, R. E. N.; Wardenburg, J. B. Staphylococcus Aureus and the Skin: A Longstanding and Complex Interaction. *Skinmed* **2015**, *13*, 111–119.
(16) Elisabeth, H.; Warren, R.; An, D. B.; Sylvain, G.; Gerard, L.; Oana, D. The Role of Antibiotics in Modulating Virulence in Staphylococcus Aureus. *Clin. Microbiol. Rev.* **2017**, *30*, 887–917. https://doi.org/10.1128/cmr.00120-16.
(17) Peterson, J. C.; Durkee, H.; Miller, D.; Maestre-Mesa, J.; Arboleda, A.; Aguilar, M. C.; Relhan, N.; Flynn, H. W. J.; Amescua, G.; Parel, J.-M.; Alfonso, E. Molecular Epidemiology and Resistance Profiles among Healthcare- and Community-Associated Staphylococcus Aureus Keratitis Isolates. *Infect. Drug Resist.* **2019**, *12*, 831–843. https://doi.org/10.2147/IDR.S190245.
(18) Sharma, B.; Kaur, G.; Chaudhary, G. R. Optimization and Utilization of Single Chain Metallocatanionic Vesicles for Antibacterial Photodynamic Therapy (APDT) against E. Coli. *J. Mater. Chem. B.* **2020**, *8*, 9304–9313. https://doi.org/10.1039/D0TB01551B.
(19) Slavkova, M.; Tzankov, B.; Popova, T.; Voycheva, C. Gel Formulations for Topical Treatment of Skin Cancer: A Review. *Gels.* **2023**, *9*, 352. https://doi.org/10.3390/gels9050352.
(20) Helal, D. A.; El-Rhman, D. A.; Abdel-Halim, S. A.; El-Nabarawi, M. A. Formulation and Evaluation of Fluconazole Topical Gel. *Int. J. Pharm. Pharm. Sci.* **2012**, *4*, 176–183.
(21) Zhao, D.; Tao, W.; Li, S.; Li, L.; Sun, Y.; Li, G.; Wang, G.; Wang, Y.; Lin, B.; Luo, C. Light-Triggered Dual-Modality Drug Release of Self-Assembled Prodrug-Nanoparticles for Synergistic Photodynamic and Hypoxia-Activated Therapy. *Nanoscale horizons* **2020**, *5* (5), 886–894.
(22) Jones, C. D.; Steed, J. W. Gels with Sense: Supramolecular Materials That Respond to Heat, Light and Sound. *Chem. Soc. Rev.* **2016**, *45*, 6546–6596. https://doi.org/10.1039/C6CS00435K.
(23) Rodrigues, M.; Calpena, A. C.; Amabilino, D. B.; Garduño-Ramírez, M. L.; Pérez-García, L. Supramolecular Gels Based on a Gemini Imidazolium Amphiphile as Molecular Material for Drug Delivery. *J. Mater. Chem. B* **2014**, *2*, 5419–5429. https://doi.org/10.1039/C4TB00450G.
(24) Fang, X.-J.; Wang, L.; Zhou, N.; Ruan, Y.-R.; Xiong, R.-Y.; Wang, Z.; Wang, W. Supramolecular Photosensitizer-Loaded Spray Hydrogel for Antibacterial Photodynamic Therapy. *ACS Appl. Polym. Mater.* **2024**, *6*, 13341–13349. https://doi.org/10.1021/acsapm.4c02722.
(25) Zhang, Y.; Zhang, H.; Zou, Q.; Xing, R.; Jiao, T.; Yan, X. An Injectable Dipeptide–Fullerene Supramolecular Hydrogel for Photodynamic Antibacterial Therapy. *J. Mater. Chem. B.* **2018**, *6*, 7335–7342. https://doi.org/10.1039/C8TB01487F.
(26) Xie, Y.-Y.; Zhang, Y.-W.; Liu, X.-Z.; Ma, X.-F.; Qin, X.-T.; Jia, S.-R.; Zhong, C. Aggregation-Induced Emission-Active Amino Acid/Berberine Hydrogels with Enhanced Photodynamic Antibacterial and Anti-Biofilm Activity. *Chem. Eng. J.* **2021**, *413*, 127542. https://doi.org/https://doi.org/10.1016/j.cej.2020.127542.
(27) Li, X.; Lee, S.; Yoon, J. Supramolecular Photosensitizers Rejuvenate Photodynamic Therapy. *Chem. Soc. Rev.* **2018**, *47*, 1174–1188. https://doi.org/10.1039/C7CS00594F.
(28) Zhao, W.; Zhao, Y.; Wang, Q.; Liu, T.; Sun, J.; Zhang, R. Remote Light-Responsive Nanocarriers for Controlled Drug Delivery: Advances and Perspectives. *Small.* **2019**, *15*, 1903060. https://doi.org/10.1002/smll.201903060.
(29) Roy, I.; Bobbala, S.; Young, R. M.; Beldjoudi, Y.; Nguyen, M. T.; Cetin, M. M.; Cooper, J. A.; Allen, S.; Anamimoghadam, O.; Scott, E. A. A Supramolecular Approach for Modulated Photoprotection, Lysosomal Delivery, and Photodynamic Activity of a

Photosensitizer. *J. Am. Chem. Soc.* **2019**, *141*, 12296–12304. https://doi.org/10.1021/jacs.9b03990.
(30) Samperi, M.; Limón, D.; Amabilino, D. B.; Pérez-García, L. Enhancing Singlet Oxygen Generation by Self-Assembly of a Porphyrin Entrapped in Supramolecular Fibers. *Cell Reports Phys. Sci.* **2020**, *1*, 100030. https://doi.org/10.1016/j.xcrp.2020.100030.
(31) Smith, S. M.; Abelha, T. F.; Limón, D.; Samperi, M.; Sharma, B.; Plaetzer, K.; Dumoulin, F.; Amabilino, D. B.; Pérez-García, L. Supramolecular and Base-Induced Singlet Oxygen Generation Enhancement of a Water-Soluble Phthalocyanine. *J. Porphyr. Phthalocyanines* **2023**, *27*, 434–443. https://doi.org/10.1142/S1088424623500128.
(32) Casal-Dujat, L.; Rodrigues, M.; Yague, A.; Calpena, A. C.; Amabilino, D. B.; Gonzalez-Linares, J.; Borras, M.; Perez-Garcia, L. Gemini Imidazolium Amphiphiles for the Synthesis, Stabilization, and Drug Delivery from Gold Nanoparticles. *Langmuir* **2012**, *28*, 2368–2381.
(33) Calpena, A. C.; Elvira, E.; San Martin, H.; Lauroba, J.; Obach, R.; Domenech, J. Influence of the Formulation on the in Vitro Transdermal Penetration of Sodium Diclofenac. *Arzneimittelforschung* **1999**, *49*, 1012–1017.
(34) Chairatana, P.; Zheng, T.; Nolan, E. M. Targeting Virulence: Salmochelin Modification Tunes the Antibacterial Activity Spectrum of β-Lactams for Pathogen-Selective Killing of Escherichia Coli. *Chem. Sci.* **2015**, *6*, 4458–4471. https://doi.org/10.1039/C5SC00962F.
(35) Samperi, M.; Pérez-García, L.; Amabilino, D. B. Quantification of Energy of Activation to Supramolecular Nanofibre Formation Reveals Enthalpic and Entropic Effects and Morphological Consequence. *Chem. Sci.* **2019**, *10*, 10256–10266. https://doi.org/10.1039/C9SC03280K.
(36) Samperi, M.; Bdiri, B.; Sleet, C. D.; Markus, R.; Mallia, A. R.; Pérez-García, L.; Amabilino, D. B. Light-Controlled Micron-Scale Molecular Motion. *Nat. Chem.* **2021**, *13*, 1200–1206. https://doi.org/10.1038/s41557-021-00791-2.
(37) Iida, S.; Ohkubo, Y.; Yamamoto, Y.; Fujisawa, A. Parabanic Acid Is the Singlet Oxygen Specific Oxidation Product of Uric Acid. *J. Clin. Biochem. Nutr.* **2017**, *61*, 169–175. https://doi.org/10.3164/jcbn.17-24.
(38) Sharma, B.; Kaur, G.; Chaudhary, G. R.; Gawali, S. L.; Hassan, P. A. High Antimicrobial Photodynamic Activity of Photosensitizer Encapsulated Dual-Functional Metallocatanionic Vesicles against Drug-Resistant Bacteria S. Aureus. *Biomater. Sci.* **2020**, *8*, 2905–2920. https://doi.org/10.1039/D0BM00323A.
(39) Tavares, T. D.; Antunes, J. C.; Padrão, J.; Ribeiro, A. I.; Zille, A.; Amorim, M. T. P.; Ferreira, F.; Felgueiras, H. P. Activity of Specialized Biomolecules against Gram-Positive and Gram-Negative Bacteria. *Antibiotics*. **2020**. https://doi.org/10.3390/antibiotics9060314.
(40) Wei, F.-X.; Zhou, T.-R.; Zhong, S.-W.; Deng, Y.-F.; Xu, C.-H.; Fu, L.-H.; Lin, B.-F. A Novel Starch-Based Ethanol Gel with Contact-Killing Bacteria to Cut off Contact Transmission of Bacteria. *Chem. Eng. J.* **2023**, *473*, 145434. https://doi.org/https://doi.org/10.1016/j.cej.2023.145434.
(41) Yin, J.; Meng, Q.; Cheng, D.; Fu, J.; Luo, Q.; Liu, Y.; Yu, Z. Mechanisms of Bactericidal Action and Resistance of Polymyxins for Gram-Positive Bacteria. *Appl. Microbiol. Biotechnol.* **2020**, *104*, 3771–3780. https://doi.org/10.1007/s00253-020-10525-y.
(42) Vaughan, J.; Benson, R.; Vaughan, K. 10 - Assessing the Effectiveness of Antimicrobial Wound Dressings in Vitro. *Woodhead Publishing Series in Biomaterials*. **2011**, 227–246. https://doi.org/https://doi.org/10.1533/9780857093301.2.227.

SUPPLEMENTARY MATERIAL

Supramolecular Gels for Antimicrobial Photodynamic Therapy against *E. coli* and *S. aureus*

Table S1. Summary of experimental conditions used for release studies.

Parameters	**Description**
Cell volume	5 mL
Diffusion area	0.64 cm^2
Sampling times	0 (pre-sample time point), 4, 8, 16, 32, 48 hr
Replicates	3
Membrane	Thermoscientific dialysis membrane, MWCO 10,000 Da
Stirring	600 rpm
Receptor fluid	DMSO:H_2O (1:9)
Temperature	32 $^oC \pm 0.5\ ^oC$
Donor Phase Sampling volume	300 µL
Dose	TPPP – 300 µL (1423.7 µg/mL) TCPP – 1000 µL (237.231 µg/mL) TPP-3OH – 300 µL (814.476 µg/mL) TPP-4OH – 300 µL (814.476 µg/mL)

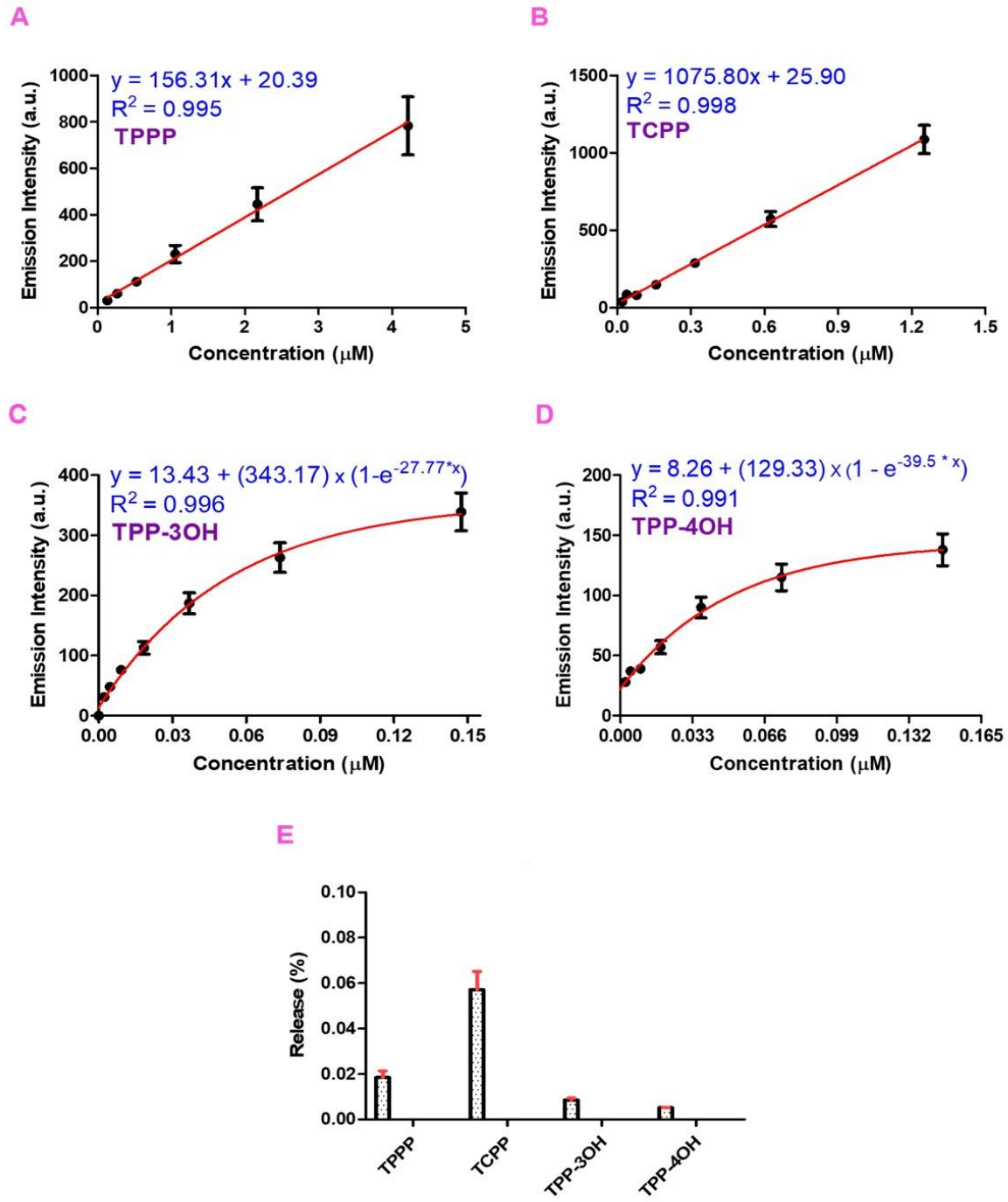

Figure S1. Calibration curves of (A) TPPP, (B) TCPP, (C) TPP-3OH, (D) TPP-4OH in DMSO:H_2O 1:9 (E) Comparison of release percentages of different porphyrins from the gel.

Table S2. Bacterial load (CFU/mL) of the inoculum before the treatment of *E. coli* and *S. aureus.*

Name of the Sample	**CFU/mL**	
	E. coli	***S. aureus***
Gel (Dark and Light)	4.7×10^{5}	2.2×10^{9}
TPPP	1.6×10^{5}	1.5×10^{9}
TCPP	7.3×10^{5}	[a]
P-OH 3’	5.0×10^{5}	[a]
P-OH 4’	4.6×10^{5}	[a]

[a] – Values not investigated

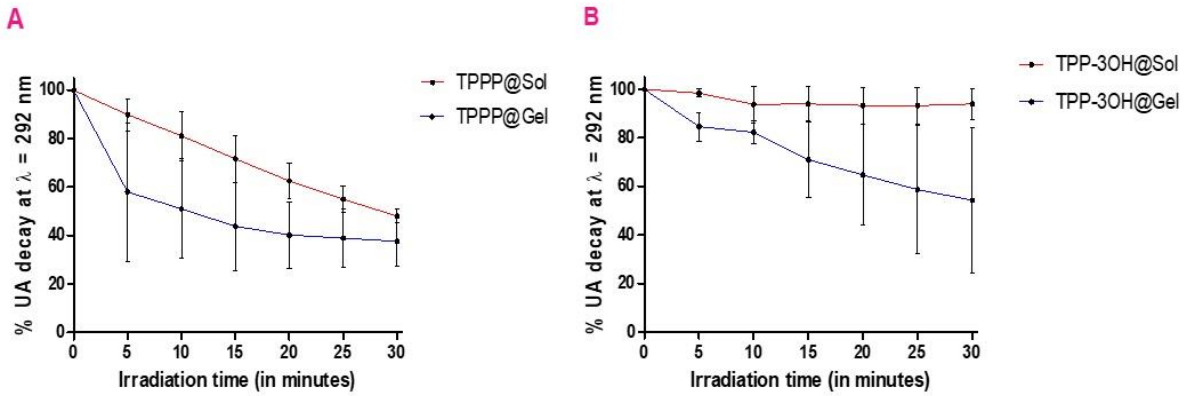

Figure S2. Percentage decrease in uric acid (UA) absorption was measured upon irradiation for the following conditions: (A) TPPP and (B) TPP-3OH, both in solution and after incorporation into the gel.

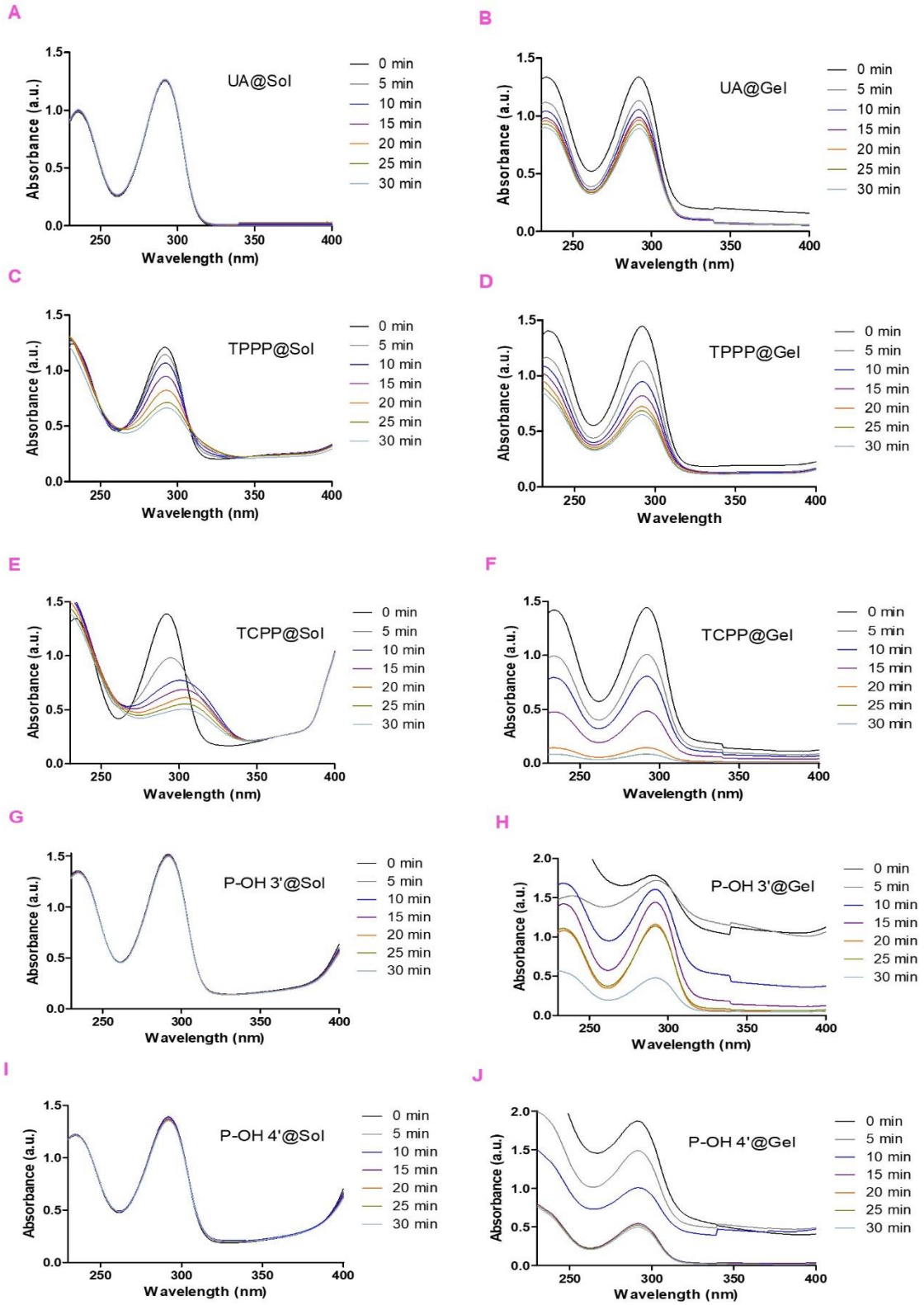

Figure S3. Absorption spectra of UA recorded upon irradiation. UA – In Sol (A) & In Gel (B), TPPP – In Sol (C) & In Gel (D), TCPP – In Sol (E) & In Gel (F), TPP-3OH – In Sol (G) & In Gel (H), TPP-4OH – In Sol (I) & In Gel (J).

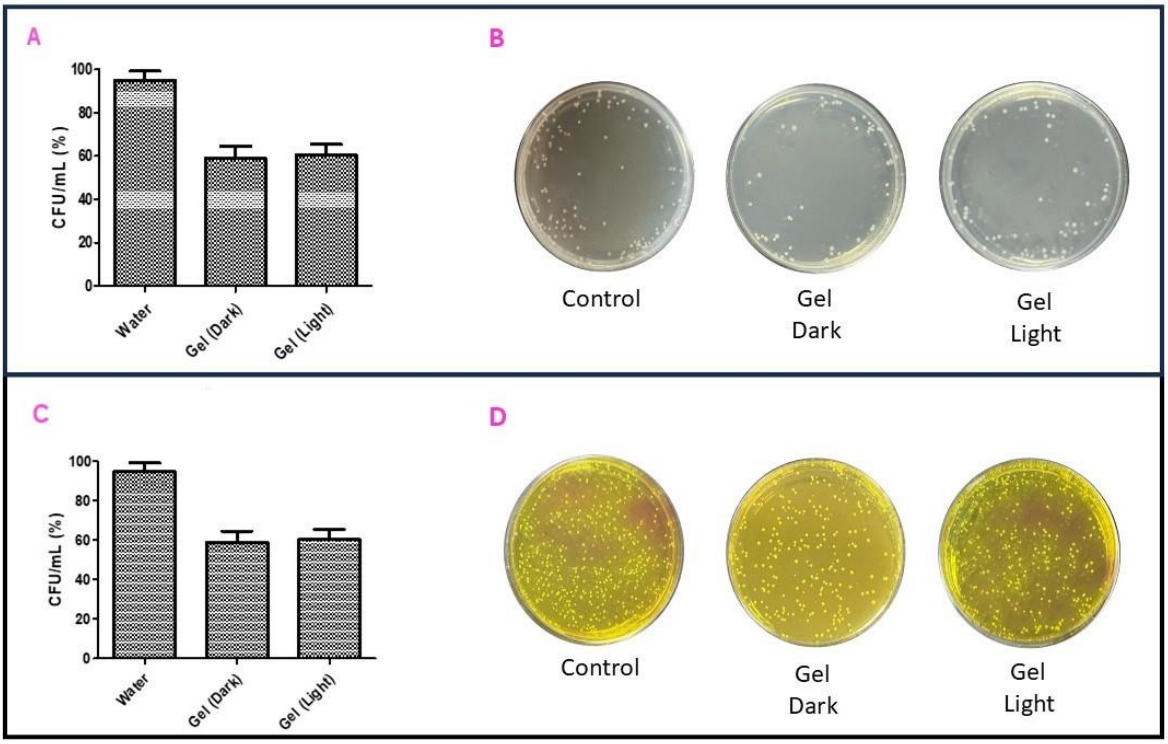

Figure S4. Graphs showing CFU/mL (%) for *E. coli* (A) Gel with and without irradiation (colony images–B), and for *S. aureus* (C) Gel with and without irradiation (colony images–D).

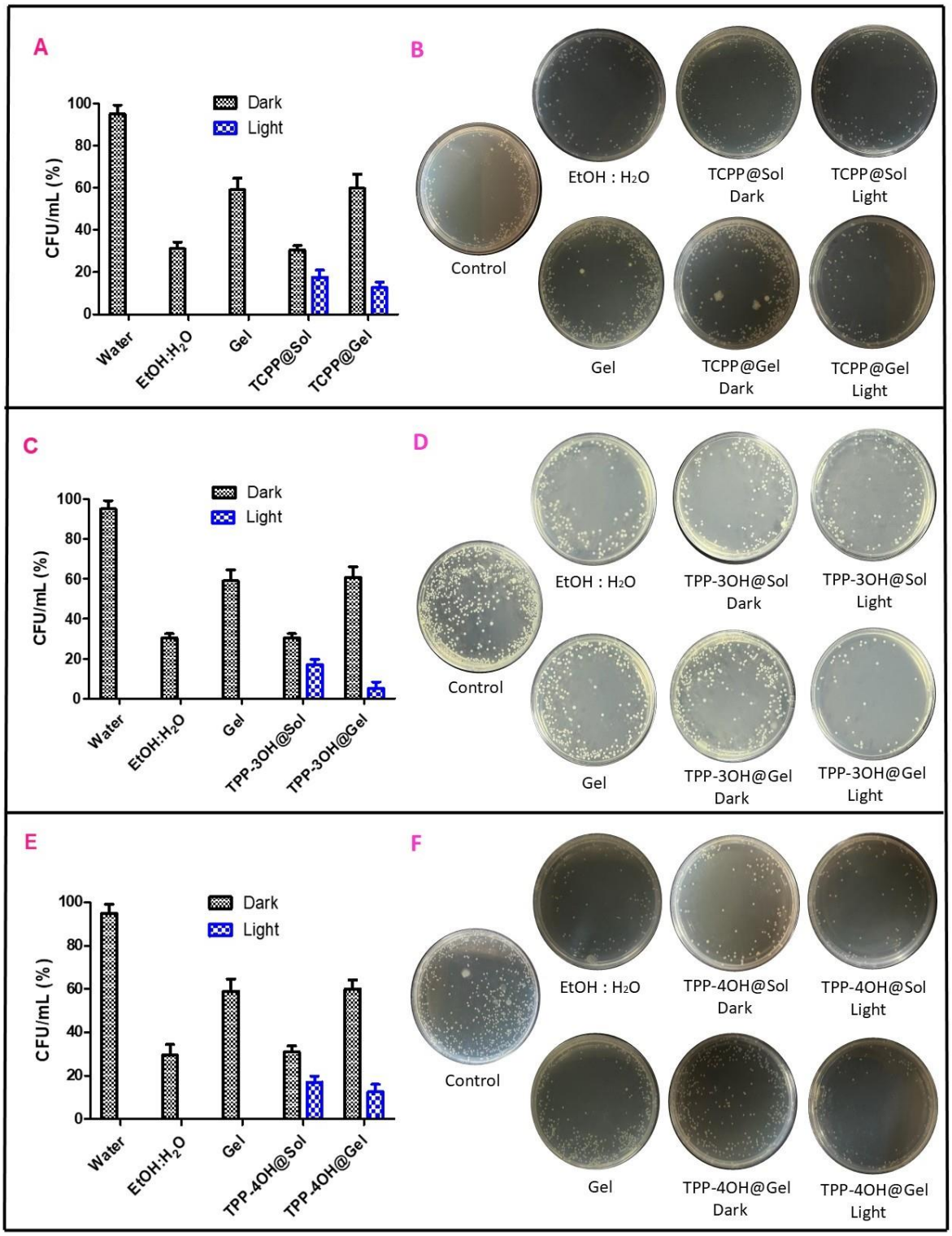

Figure S5. Graphs showing *E.coli* CFU/mL (%) plot for (A) TCPP (colony images- B), (C) TPP-3OH (colony images- D) and (E) TPP-4OH (colony images- F). The porphyrin concentration in all the gels is 25 µM.

Table S3. CFU reduction (%) when each of the photosensitizers are in solution and in the gel after irradiation for 30 minutes for both *E. coli* and TPPP for *S. aureus.*

Name of the Sample	**CFU reduction (%)**			
	E. coli			
	Dark Conditions		**Light Conditions**	
	Sol	Gel	Sol	Gel
Ethanol: Water 1:1	70	[a]	[a]	[a]
Gel	[a]	40	[a]	40
TPPP	70	40	94	97
TCPP	70	40	80	83
TPP-3OH	70	40	80	90
TPP-4OH	70	40	77	81
	S. aureus			
TPPP	70	40	100	100

[a] – Not applicable